Experimental comparison of noise and resolution for *2k* and *4k* storage phosphor radiography systems[a)]

Michael J. Flynn[b)] and Ehsan Samei[c)]

Department of Diagnostic Radiology, Henry Ford Health System, Detroit, Michigan 48202
and Department of Nuclear Engineering and Radiological Sciences,
The University of Michigan, Ann Arbor, Michigan 48109

The purpose of this study was to compare the image quality for a digital storage phosphor system using 1760×2140 ($2k$) and 3520×4280 ($4k$) image arrays. Measurements were made on a chest radiography system (Fuji FCR-9501) with special provisions to be operated in both $2k$ (standard) and $4k$ (HQ) modes. Presampled modulation transfer functions (MTF) were measured using an edge method. Noise power spectra (NPS) were determined for different input exposures by two-dimensional Fourier analysis. These measures along with exposure measurements and an x-ray spectral model were used to determine the frequency-dependent detective quantum efficiency DQE (f) of the system for the $4k$ and the $2k$ modes. The magnitude of the NPS for the $4k$ mode was about 1/2 that of the $2k$ mode. A MTF value of 0.5 was found at 1.25 cycles/mm for the $4k$ system and 1.50 cycles/mm for the $2k$ system. The $4k$ images had an extended MTF of 0.1 at 4.5 cycles/mm in the plate-scan direction. Overall, the DQE (f) of the $4k$ mode was slightly better than that for the $2k$ mode by about 0.02 due primarily to its better noise characteristics. © *1999 American Association of Physicists in Medicine.* [S0094-2405(99)00408-3]

I. INTRODUCTION

Digital storage phosphor (DSP) radiography, commonly known as computed radiography (CR), is now widely used to acquire digital radiographs. DSP image quality depends on the radiation detection properties of the storage phosphor screen, the light diffusion associated with reading the screen with a scanned laser beam, and signal processing associated with electronic signal acquisition components. A number of improvements in DSP screens and instrumentation for reading screens have been introduced since earlier reports of DSP image quality were published.[1–5] We report in this paper the measured image quality of a DSP instrument with features for scanning 35 by 43 cm phosphor screens with 100 μm pixels (3520×4280 array size) rather than with standard 200 μm pixels (1760×2140 array size). This work was largely motivated by a desire to understand the relative performance of $2k$ and $4k$ DSP systems for chest radiography.

Since the first introduction of DSP systems, instruments of various manufacturers have used DSP screens fabricated by Fuji Medical Systems. As these screens have been improved, they have been designated as type I, II, III, and V screens.[6] The performance of earlier type screens with respect to their measured modulation transfer function (MTF), noise power spectrum (NPS), and detective quantum efficiency (DQE) was recently reported.[7] This report provides similar information for type ST-Va screens and a reader of a more advanced design.

The MTF provides a convenient description of a system's resolution. It has been most commonly measured using slit test devices to estimate the line spread function from which the MTF can be computed.[8–10] Equivalent measures can be made with devices designed for measurement of the point spread function, edge spread function, or with devices having periodic patterns of varying spatial frequency. For this work, we have used a method utilizing an edge test device. The details of this method have been described in a recent paper where it is shown to be equivalent to slit methods used by other investigators.[11]

Similarly, the NPS provides a convenient description of the noise amplitude and texture observed in images obtained with a uniform field of radiation having a specific fluence and spectral quality. The noise of images recorded on film has been commonly analyzed from signals obtained using a scanning densitometer with a slit aperture.[12] The NPS is computed as a one-dimensional power spectrum describing noise amplitude and correlation in the direction of the scan. This method has been extended for application to digital images.[13] In two recent articles,[7,14] the NPS has been computed from digital images using a two-dimensional (2D) Fourier transform to obtain a 2D NPS describing the noise correlation at all orientations in the image. For this work, we have similarly used a 2D Fourier transformation method. However, the method is distinctly different from previous approaches with respect to specific processes such as the elimination of the background signal, processing of the data in relative noise units, and the spectral estimation filter. The details of our NPS analysis are reported in this paper.

The DQE is typically used to describe the efficiency of a

TABLE I. Specifications of acquisition modes of FCR-9501 and FCR-9501-HQ systems.

Image size (cm^2)	Mode	Digital matrix	Pixel size (μm)	Limiting frequency (cycles/mm)	Image size (Mbytes)
35×43	HQ	3520×4280	100	5.0	30.1
35×43	ST	1760×2140	200	2.5	7.5
35×35	ST	1760×1760	200	2.5	6.2
24×30	ST	1670×2010	150	3.3	6.7
18×24	ST	2000×2510	100	5.0	10.0

system recording a monoenergetic radiation beam.[15] Estimates of this function can be made using a heavily filtered x-ray beam. To determine the DQE, it is necessary to estimate the ideal noise equivalent quanta (NEQ) for the x-ray beam. Recent reports of system DQE measured with a broad radiation spectrum have used estimates of the total quanta in the x-ray beam.[7,14] In this work, we define the ideal NEQ as the square of the signal-to-noise ratio which would be observed with a detector behaving as an ideal integrator of input x-ray energy.[2] The signal and noise of the ideal detector are deduced from integrals which depend on an estimate of the x-ray spectrum.

II. METHODS

All measurements were performed on an FCR-9501/FCR-9501-HQ DSP device manufactured by Fuji Medical Systems. The reader is the same device as is employed in the Fuji 9000 series of devices designed for use with cassettes. The FCR-9501 system, intended for use in upright chest examinations, has four 35×43 cm screens which are rotated into position for exposure and directly transported to the laser scanning device which reads the stored signal. All measurements were performed with the antiscatter grid removed and comparative results were associated with data from the same phosphor screen.

The FCR-9501 produces digital images with an array size of 1760×2140 pixels where each pixel is 200 μm in size for the 35×43 cm field size. Table I summarizes the sizes for some other modes of the system. An alternate system, the FCR-9501-HQ, produces an array of 3520×4280 pixels where each pixel is 100 μm in size for the 35×43 cm field size. The DSP system used for this work was set up by Fuji Medical Systems with a special provision to allow the system to be operated as either FCR-9501 or FCR-9501-HQ. This was accomplished by turning the system off, changing a programed memory card internal to the electronic portion of the system, and restarting the system. It was then necessary to change configuration parameters in both the laser film printer (Fuji, FILM-D) and the quality assurance workstation (Fuji, HIC-654) to support the pixel size mode of the reader.

All images acquired from the DSP system were sent to the attached workstation (HIC-654) using a high-speed digital connection. Images in a proprietary format were then transferred to a Unix workstation using a high-speed digital transfer device (DASM-FDLR, Analogics, Inc.). The images were converted from the raw DSP format used by Fuji Medical Systems, which is in proportion to the logarithm of the re-

corded signal, to a 16 bit integer number which was linearly proportional to the recorded signal and stored in a generic image format used in our research laboratory. The image conversion was done using the relationship

$$I(j,k) = 10^{Q(j,k)L/1024}, \tag{1}$$

where $Q(j,k)$ is the DSP signal array (10 bit numbers ranging from 0 to 1023), $I(j,k)$ is the linear signal array, and j and k are the row and column indices for the digital image. For this work, the rows are associated with the laser scan or x direction and the columns are associated with the plate scan or y direction. The latitude L was set to be equal to 2.0 when acquiring data for both the MTF and the NPS analyses.

All radiographic exposures were made using a high-frequency x-ray generator (ACOMA 1050 HF) whose high-voltage accuracy had been verified to be within 2 kV. The x-ray tube with added filtration produced a radiation beam with a half-value layer (HVL) of 4.41 mm aluminum at a nominal 120 kV$_p$. All measurements were made with a nominal 0.3 mm focal spot (0.5 mm measured) and a focal spot to DSP phosphor distance of 183 cm. Data were acquired using high-voltage values of 70, 115, and 150 kV$_p$, all with 19 mm of additional aluminum filtration (type 1100) at the collimator. An additional 1 mm of copper was added to the filtration for the 150 kV$_p$ measurements. These test conditions produced radiation spectra with estimated aluminum HVL values of 6.3, 9.5, and 13.3 mm, respectively.

Data were acquired to document the MTF, NPS, and DQE of the system operating in both 100 μm ($2k$) and 200 μm ($4k$) modes at 70, 115, and 150 kV$_p$. Additional data were acquired to establish the variation of NPS with exposure and the repeatability of measurements at 115 kV$_p$. The specific methods for MTF, NPS, and DQE determination are described in the following sections.

A. Modulation transfer function

All MTF measurements were made with an edge test device constructed of a 0.25-mm-thick lead foil having a precision-polished edge. The MTF measurements corresponding to the resolution in the laser-scan direction were made with the edge oriented nearly parallel to the plate-scan direction. Similarly, the plate-scan MTF measurements were made with the edge oriented nearly parallel to the laser-scan direction. Measurements were made with a small focal spot and the test device near the DSP phosphor to eliminate any geometric blur.
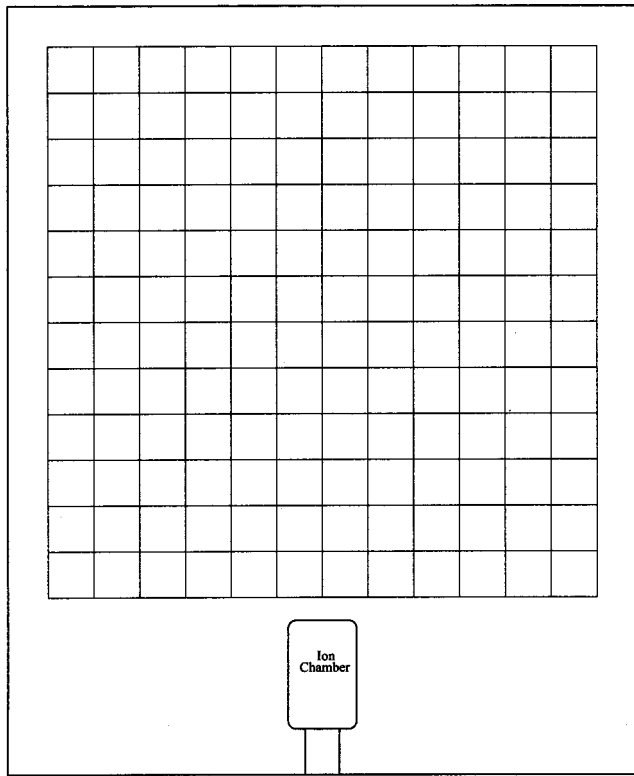
FIG. 1. The division of the radiographs into 144 subarrays in each of which the 2D NPS was computed by FFT. The results were then normalized and averaged to obtain the NPS of the system. The image array and subarray sizes were 1760×2140 and 128×128 for the FCR-9501 system, and 3520 ×4280 and 256×256 for the FCR-9501-HQ system.

The methods used to process the recorded 2D image of the edge to obtain the presampled MTF have been described in a recent publication.[11] In summary, the angle of the edge was determined with high accuracy using a Hough transformation.[16] The 2D data in the region of the edge were then reprojected into one-dimensional estimates of the edge spread function (ESF) with 0.1 pixel increments. The ESF was smoothed and differentiated using a central difference algorithm. Finally, the presampled MTF was determined by Fourier transformation. This method yields the MTF for the laser-scan direction and for the plate-scan direction at discrete spatial frequencies, $MTF(n)$ and $MTF(m)$.

B. Noise power spectrum

NPS measurements were made by exposing the DSP screen to a uniform beam of radiation while simultaneously measuring the radiation exposure in the lower portion of the field. Within the acquired digital image array, a set of small image subarrays arranged contiguously in 12 columns and 12 rows were identified (see Fig. 1) and the two-dimensional NPS determined for each subarray. For the 1760×2140 arrays of 200 μm pixels ($2k$), the subarray size was 128×128 ($N=128$). For the 3520×4280 arrays of 100 μm pixels ($4k$), the subarray size was 256×256 ($N=256$). Using the assumption that the NPS is inversely proportional to the radiation fluence incident on the subarray region, and hence

the mean signal within a subarray, the NPS of each subarray was scaled to the incident fluence of the upper left subarray. Specifically, the NPS values were divided by the ratio of the mean value for the subarray to the mean value for the upper left subarray. The average of the NPS for all subarrays was then computed.

The radiation exposure associated with the NPS image was measured using an ionization chamber placed approximately equidistant from the DSP screen and the x-ray tube focal spot. The exposure incident on the screen was then estimated using the inverse-square law. This exposure was linearly scaled by the ratio of the mean signal in the upper-left subarray to the mean signal in the region of the image surrounding the recorded pattern of the ion chamber in order to correct for large-scale nonuniformities in the image such as those caused by the heel effect. The exposure that we report is thus that which would be present at the upper-left subarray position of the screen if the screen were not present. This measurement, therefore, does not include any contribution from radiation scattered within the DSP system.

Within each subarray, the data were first corrected for nonuniformity and scaled in value. The stochastic noise associated with quantum mottle is superimposed on a fixed pattern, which may reflect beam nonuniformity associated with the heel effect or low-frequency noise associated with the DSP instrumentation. For each of s subarrays, $I_s(j,k)$, the low-order signal associated with these fixed patterns was removed by obtaining the coefficients of a two-dimensional function having the form

$$I_{s,fit}(j,k) = C_1 + C_2 j + C_3 k + C_4 j^2 + C_5 k^2 + C_6 jk, \qquad (2)$$

from a least-squares regression analysis. This function was then subtracted from the data within the subarray:

$$\Delta_s(j,k) = I_s(j,k) - I_{s,fit}(j,k). \qquad (3)$$

This estimate of the stochastic variations was then normalized by the mean value $\bar{I}_s$ of the data within the subarray:

$$\delta_s(j,k) = \frac{\Delta_s(j,k)}{\bar{I}_s}. \qquad (4)$$

Normalization of the image noise to relative noise values removes the signal units of the DSP data and facilitates evaluation of the NPS. We note here that the mean-square value of $\delta_s(j,k)$ is equal to the relative noise variance of the image:

$$\sigma_\delta^2 = \left(\frac{\sigma_{I_s}}{\bar{I}_s}\right)^2 = \frac{1}{N^2} \sum_{j=1}^{N} \sum_{k=1}^{N} \delta_s^2(j,k). \qquad (5)$$

For counting detectors and uncorrelated Poisson noise, this relative noise variance is equal to the reciprocal of the average number of quanta counted in each pixel:

$$\left(\frac{\sigma_{I_s}}{\bar{I}_s}\right)^2 = \frac{1}{\Phi_p}, \qquad (6)$$

where Φ_p is the detected fluence, or noise equivalent fluence, in quanta/pixel. We, therefore, have also scaled the relative noise by the area associated with each pixel of the acquired image array:

$$\delta_s'(j,k) = a_p^{1/2} \delta_s(j,k), \tag{7}$$

where $a_p = x_p \times y_p$ is the area associated with an image pixel. For this work, the pixel dimensions in the laser-scan and the plate-scan direction were equal ($x_p = y_p$). $\delta_s'(j,k)$ is thus consistent with the concept of noise equivalent to a counting detector and produces a relative noise variance with units equivalent to $1/(\text{quanta/mm}^2)$ rather than $1/(\text{quanta/pixel})$. This normalization of the relative noise by pixel area produces the desired units for the NPS following Fourier transformation (see the appendix).

Prior to Fourier transformation, $\delta_s'(j,k)$ was modified by multiplying the subarray values by a Hamming window function of the type commonly used in spectral estimation,[16]

$$\delta_s''(j,k) = \delta_s'(j,k) H(r), \quad \text{for } r < \frac{N}{2}, \tag{8}$$

where

$$H(r) = 0.54 + 0.46 \cos(\pi r), \tag{9}$$

and

$$r^2 = \left(i - \frac{N}{2}\right)^2 + \left(j - \frac{N}{2}\right)^2. \tag{10}$$

Outside of the circular region with diameter N, $\delta_s''(j,k)$ was set to zero. The Hamming window function was normalized such that the mean-square value of $H(r)$ was 1.0 in order to preserve the magnitude of the NPS. Use of this window function eliminates aliasing from discontinuities at the edge of the subarray (-40 db sidelobe) and provides some spectral smoothing (spectral width of 2 pixels in the frequency domain).

Finally, the Fourier transform of the windowed subarray data $\eta_s(n,m)$ was computed (see the appendix) and the noise power spectrum expressed as the square of the complex magnitude:

$$\text{NPS}_s(n,m) = |\eta_s(n,m)|^2. \tag{11}$$

$\text{NPS}_s(n,m)$ was determined in this manner for each subarray and the results for all subarrays were combined as described above to determine an average noise power spectrum for the screen tested:

$$\text{NPS}(n,m) = \frac{1}{144} \sum_{s=1}^{144} \text{NPS}_s(n,m) \frac{\bar{I}_s}{\bar{I}_1}, \tag{12}$$

where $s = 1$ corresponds to the reference subarray in the upper-left corner of the image. For convenience, $\text{NPS}(n,m)$ was stored in an $N \times N$ array with the value associated with zero frequency at $(N/2, N/2)$ and maximum frequencies at $n = N$ and $m = N$ of $1/2x_p$ and $1/2y_p$ cycles/mm. The noise power spectra in the laser-scan direction and in the plate-

scan direction, NPS(n) and NPS(m), were estimated by averaging the central row or column and ± 5 rows or columns within the 2D NPS array.[7]

All processes associated with our NPS estimation algorithm were verified by generating an image with a mean value of 1000 for each pixel and with random noise added to each pixel corresponding to a Poisson distribution with a mean of 1000. Using a pixel area of 0.04 mm^2 (i.e., 200 μm pixel size), the noise power spectrum was correctly computed with a near-constant value of 4×10^{-5} mm^2 at all frequencies corresponding to uncorrelated noise with a noise equivalent quanta of 25 000 quanta/mm^2 (see the appendix).

C. Detective quantum efficiency

The DQE for the laser-scan direction was computed using the relationship

$$\text{DQE}(n) = \frac{\text{NEQ}(n)}{q} \tag{13}$$

and

$$\text{NEQ}(n) = \frac{[\text{MTF}(n)]^2}{\text{NPS}(n)}, \tag{14}$$

where MTF(n) is the modulation transfer function, NPS(n) is the noise power spectrum measured at a given exposure, q is the square of the ideal signal-to-noise (SNR) ratio, and NEQ(n) is the noise equivalent quanta. The values of MTF(n) were linearly interpolated to obtain frequency increments equivalent to the NPS. Similar equations were used to compute the DQE for the plate-scan direction, DQE(m).

This definition for DQE is equivalent to conventional formulations,[15] which approximate nonlinear signals as locally linear with a gain associated with the slope of the response curve [i.e., $S = G \log(E)$ and $\Delta S \approx G \Delta Ei$, where $S = $ signal, $E = $ exposure, and $G = $ gain]. Since our image values were initially transformed to a linear signal, the gain term equals 1.0. For the DQE calculations, the presampled MTF was used as opposed to the aliased, expected MTF (EMTF), as suggested by Dobbins.[17]

The ideal SNR^2 was defined for an ideal detector which perfectly integrates the full energy of each incident photon. A semiempirical x-ray spectra model, based on earlier work by Storm,[18,19] was used for the calculations at three kV$_p$ (70, 115, and 150) accounting for both characteristic x-ray and bremsstrahlung radiation. The ideal SNR^2 per unit exposure was then calculated from the first and the second moment of the energy spectrum.[2] q was then determined by multiplying the measured exposure by the estimated values for the ideal SNR^2 per unit exposure. Exposures were measured free in air at a 102 cm distance from the focal spot and the exposure incident on the screen at 183 cm from the focal spot was estimated using the inverse-square law.

Figure 2 shows the modeled spectra used to carry out the calculations. The accuracy of the spectral model used to estimate q was verified using experimental measurements of exposure and the half-value layer made using additional filtration of 1.9 cm aluminum, for 70 and 115 kV$_p$, and 1.9 cm
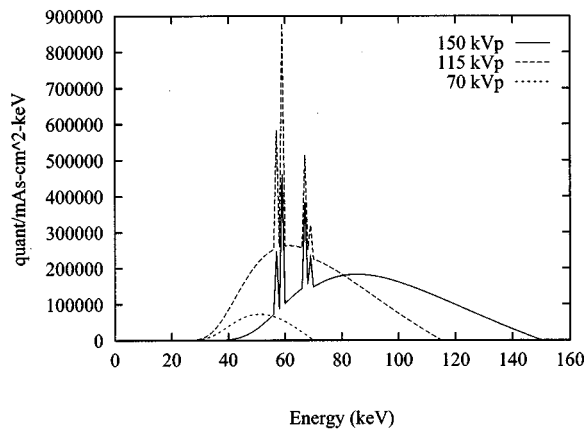
FIG. 2. The spectra for the 70, 115, and 150 kV$_p$ x-ray beams computed by the spectral model. Added filtrations for the three kV$_p$ were 1.9 cm Al, 1.9 cm Al, and 1.9 cm Al/1 mm Cu, respectively. The spectra for 115 and 150 kV$_p$ are seen to be broad and asymmetric. The ideal SNR^2 was computed from these spectra assuming an ideal energy-integrating detector.

aluminum/1 mm copper, for 150 kV$_p$. The agreement was within 6%. Using these spectra, the ideal SNR^2 per unit exposure was estimated to be 261 579 quanta/mm^2 mR for the 70 kV$_p$ beam, 264 580 quanta/mm^2 mR for the 115 kV$_p$ beam, and 231 321 quanta/mm^2 mR for the 150 kV$_p$ beam. No smoothing was applied to the estimated DQEs.

III. RESULTS

In order to allow convenient comparison between various performance measures as they relate to specific questions about the system and the measurement methods, the results are organized into four subsections. The following subsections report on the MTF, NPS, and DQE results, focusing on the $4k$ and the $2k$ image acquisition modes, on directional dependencies, and on variations as a function of kV$_p$. Reproducibility of the measurements is reported in the final section.

A. $4k$ versus $2k$ modes

Figures 3(a) and 3(b) show the presampled MTF for the $4k$ and $2k$ modes in the laser-scan (LSC) and the plate-scan (PSC) directions. The measurements were acquired at 115 kV$_p$. The $4k$ mode, as compared to the standard $2k$ mode, offers a slightly improved response at spatial frequencies above 2.5 cycles/mm at the expense of a diminished response at lower frequencies, especially in the plate-scan direction. The noise and anomalous peaks at high frequencies in the measured MTF for the $2k$ mode may be attributed in
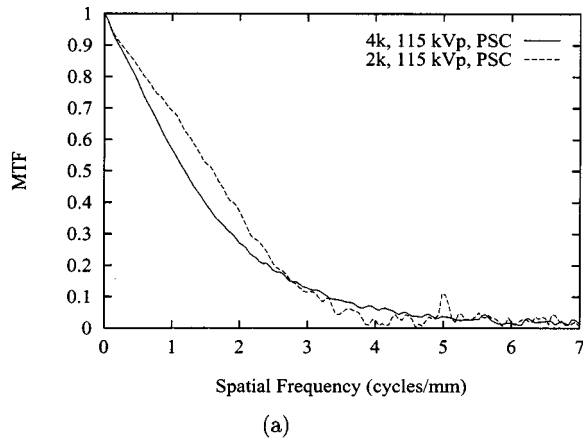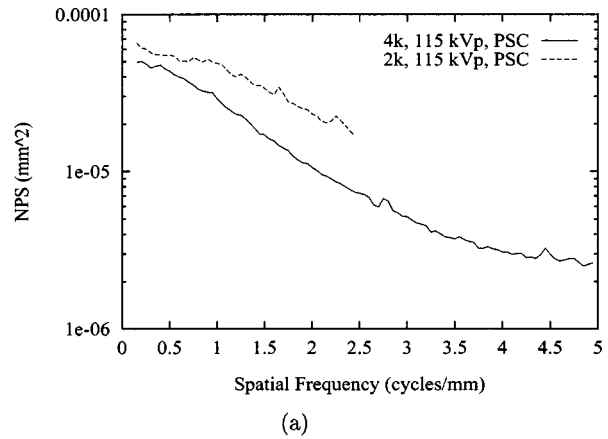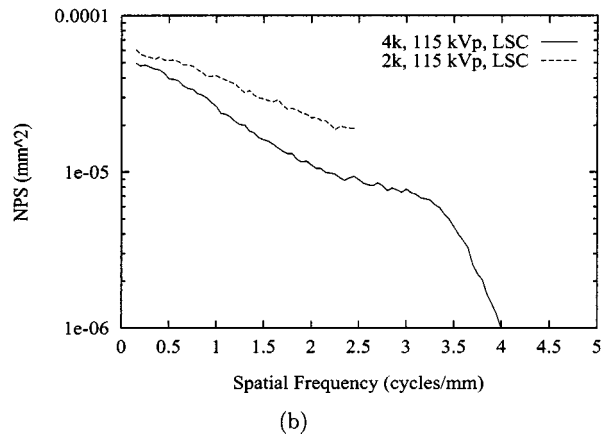

(a)
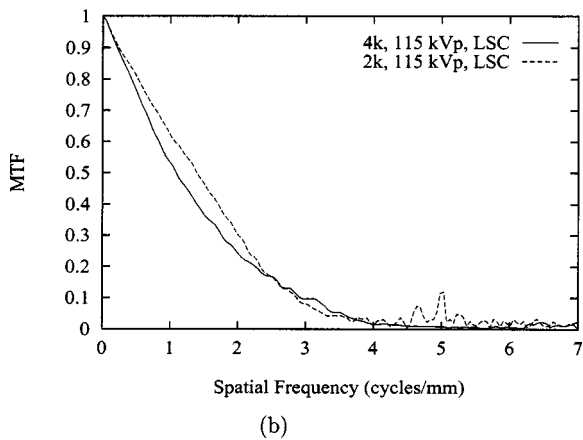
(b)

FIG. 3. The presampled MTF measured at 115 kV$_p$ for the $4k$ and $2k$ modes in the plate-scan (a) and the laser-scan (b) directions.
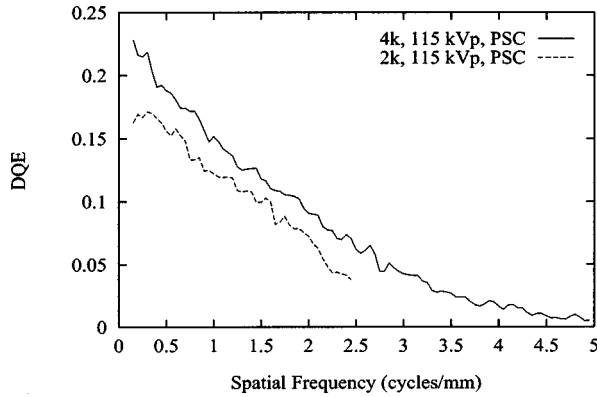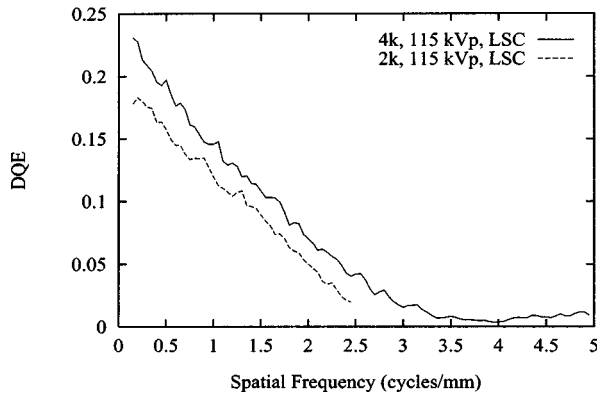

(a)

(b)

FIG. 4. The NPS measured at 115 kV$_p$ for the $4k$ and $2k$ modes in the plate-scan (a) and the laser-scan (b) directions. The data were acquired at an exposure of 0.3 mR to the phosphor screen.

FIG. 5. The DQE determined at 115 kV$_p$ for the $4k$ and $2k$ modes in the plate-scan (a) and the laser-scan (b) directions.

part to a positive bias in the estimate of the MTF at high frequencies due to the use of both cosine and sine terms in the Fourier transformation when an edge method is used.[8]

Figures 4(a) and 4(b) show the NPS measured for the $4k$ and $2k$ modes in both directions at 115 kV$_p$. The NPS for the $4k$ mode is substantially better than that for the standard $2k$ mode. The improved noise characteristics of the $4k$ mode may be due in part to increased reading time of the phosphor screen in this mode. We measured an approximately 70% increase in the estimated reading time for the $4k$ mode as compared to the $2k$ mode. The sharp decrease in the NPS for the $4k$ mode in the laser-scan direction at about 3.2 cycles/mm is probably associated with an antialiasing filter applied in that direction.

Figures 5(a) and 5(b) illustrate the DQE of the $4k$ and $2k$ modes in both directions at 115 kV$_p$. The DQE for the $4k$ mode is consistently about 0.025 higher than that for the standard $2k$ mode in both directions within the frequency range of 0 to 2.5 cycles/mm. This difference is primarily due to the improved noise characteristics of the $4k$ mode as compared to the $2k$ mode.

B. Directional dependencies

Figure 6 shows the differences in the MTF in the laser-scan and the plate-scan directions for the $4k$ mode at 115
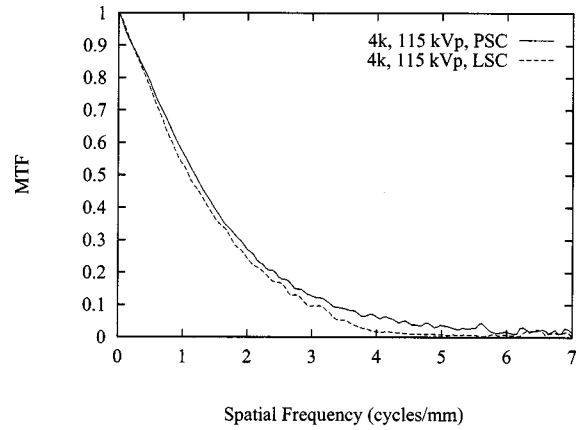

FIG. 6. The presampled MTF for the $4k$ mode at 115 kV$_p$ in the laser-scan and the plate-scan directions.

kV$_p$. The MTF measures in both directions are similar, with the response in the LSC direction being slightly lower at higher frequencies. The laser-scan MTF approaches zero at the Nyquist frequency ($f_N = 5.0$ cycles/mm) as a consequence of the antialiasing filter applied in that direction. The difference between the responses in the LSC and PSC directions has been reported to be more pronounced for earlier generations of DSP systems.[7]

Similar observations can be made in the NPS results, illustrated in Fig. 7. The NPS in the LSC direction shows a pronounced falloff at high frequencies as compared with that in the PSC direction due to the antialiasing filter in that direction. The anomalous increase in the frequency range of 2.2–3.7 cycles/mm is likely associated with the antialiasing filter. The cumulative effects of the MTF and NPS lead to a gradual falloff in the DQE for the LSC direction at higher frequencies as compared to that in the PSC direction, as illustrated in Fig. 8.
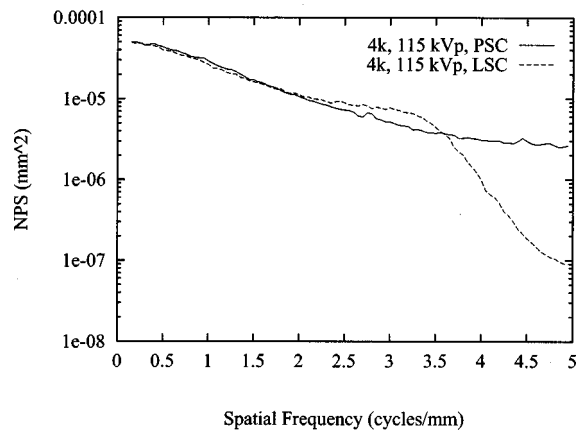

FIG. 7. The NPS for the $4k$ mode at 115 kV$_p$ in the laser-scan and the plate-scan directions using an exposure of 0.3 mR to the phosphor screen.
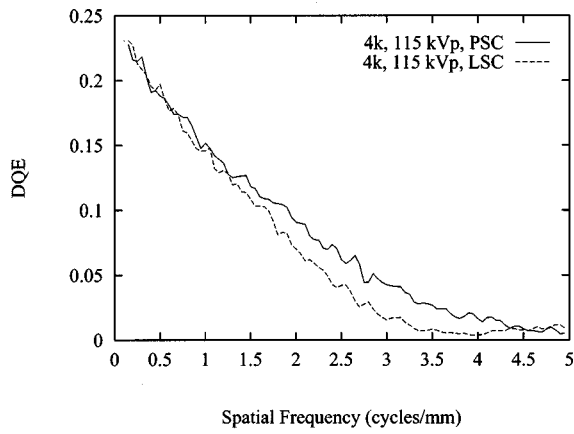
FIG. 8. The DQE for the $4k$ mode at 115 kV$_p$ in the laser-scan and the plate-scan directions.

FIG. 10. The NPS for the $4k$ mode in the plate-scan direction measured at 70, 115, and 150 kV$_p$. The measures were acquired using 0.279, 0.287, and 0.316 mR exposure to the upper-left corner of the phosphor screen.

C. Energy dependencies

The influence of the x-ray energy on the MTF is illustrated in Fig. 9. The results are obtained at three kV$_p$, 70, 115, and 150, for the $4k$ mode in the PSC direction. The results are very similar with only minute differences. The MTF measures at 115 and 150 kV$_p$ are slightly lower than that at 70 kV$_p$ by about 2% and 7%, respectively. The observed differences can be explained by the fact that higher-energy x rays deposit their energy more deeply into the phosphor screen, leading to a degradation of resolution.

Figure 10 shows the NPS as a function of kV$_p$. The NPS increases with kV$_p$. The measured NPS at 150 kV$_p$ is notably higher that those at 70 and 115 kV$_p$. Since all three measurements were acquired at the same exposure level of about 0.3 mR, the observed differences may be attributed to a lower detection efficiency of the detector for higher-energy photons as well as a decrease in the number of quanta per unit exposure as the average energy of the beam increases, considering the energy-integrating character of the detector. The variation in the measured DQE with kV$_p$ is plotted in Fig. 11. The
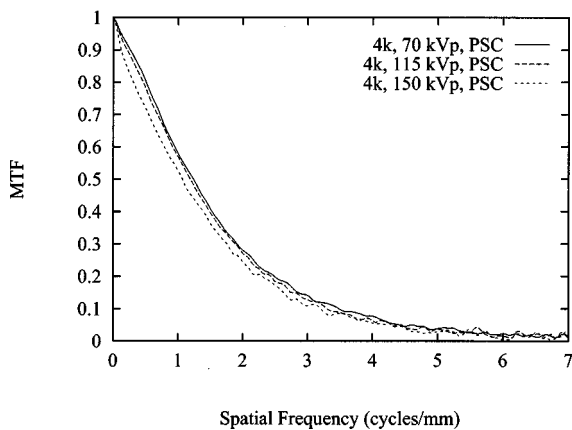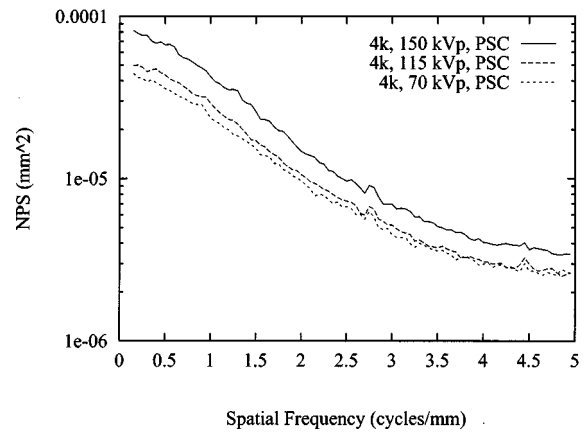
results demonstrate that the DQE is a strong function of kV$_p$, mostly due to the contribution of the NPS.

D. Reproducibility

In order to assure reproducibility in the measurement methods and performance stability of the imaging system,
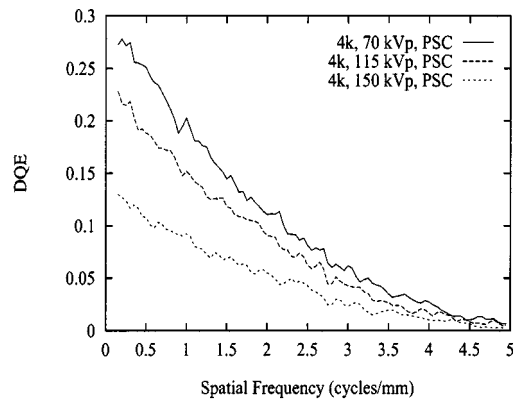
(a)

(b)

FIG. 11. The DQE for the $4k$ (a) and $2k$ (b) modes in the plate-scan direction measured at 70, 115, and 150 kV$_p$. The measures were acquired using 0.3 mR exposure to the upper-left corner of the phosphor screen.

FIG. 9. The presampled MTF for the $4k$ mode in the plate-scan direction measured at 70, 115, and 150 kV$_p$.

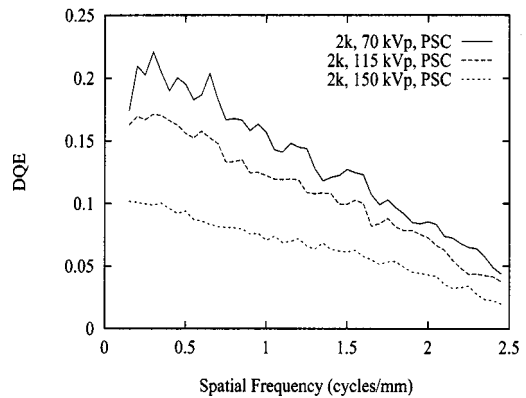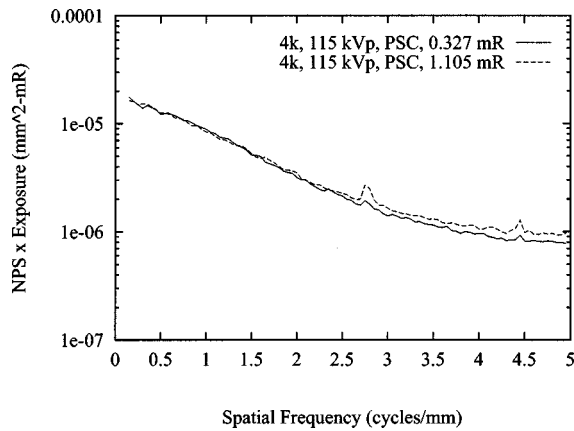FIG. 12. Verification of the exposure response for the NPS measurements. The curves show the product of NPS and exposure as a function of spatial frequency. If the noise comes only from x-ray quantum mottle, the results are expected to be identical. A small amount of instrument noise is noted at frequencies above 2.5 cycles/mm with two small peaks observed in the spectrum at 1.1 mR which are not seen in the 0.3 mR spectrum.

independent measurements of the MTF and NPS were acquired. The results of two MTF measurements for the $4k$ system at 115 kV$_p$ acquired over an interval of six months yielded essentially equivalent results. Similarly, excellent reproducibility in NPS measurements was observed using exposures of about 0.3 mR to the phosphor screen.

If the only source of noise is associated with the input radiation fluence, the NPS is expected to vary inversely with the incident exposure. To evaluate this, the NPS was measured using two different exposures at about 0.3 and 1.1 mR. The results, shown in Fig. 12, were analyzed by plotting the product of NPS and exposure. A small increase in this product is seen for an exposure of 1.1 mR relative to the result at 0.3 mR. This suggests a small component of instrument noise is present at frequencies above 2.5 cycles/mm. The DQE results were obtained at about 0.3 mR and are believed to reflect a negligible amount of instrumentation noise.

IV. DISCUSSION

Chest radiography with DSP technology is typically performed using a 200 μm pixel dimension producing an image array of approximately $2k$ for a standard 35 by 43 cm radiograph. A DSP system for chest radiography capable of producing radiographs with a pixel dimension of 100 μm in a $4k$ image array was recently introduced by one manufacturer. Intuitively, one might assume that by increasing the sampling rate (or reducing the pixel size), a higher resolution could be achieved with an adverse effect on noise. However, previous studies have reported that reducing the pixel size has not proportionally improved the resolution,[5] suggesting that the intrinsic presampled transfer characteristics of the system may not be sufficient to substantiate the resolution dictated by the sampling rate. This raises the question of whether the $4k$ system provides an improved image quality and should be preferred to the standard $2k$ acquisition mode. In this work, we addressed this question by performing a comparative quantitative assessment of image quality of a

DSP system operating in the $2k$ and the $4k$ acquisition modes in terms of the established measures for resolution, noise, and signal-to-noise ratio, i.e., MTF, NPS, and DQE.

The $4k$ system offers a limiting spatial resolution twice that of the $2k$ system (5.0 vs 2.5 cycles/mm). The measured MTF responses, however, indicate that the $4k$ system is inferior to the $2k$ system in the low- to midfrequency range. In imaging objects with significant high-frequency content, such as the skeletal extremities, a small pixel size and the high-frequency response may be preferred. However, in chest examinations, the response in the low- to midfrequency range is more important. For example, subtle lung nodules with poorly defined edges and dimensions ranging from a few to tens of millimeters (Ref. 20) do not contain high-frequency signals. Therefore, on the basis of the MTF alone, the $2k$ system seems to be a preferred system for chest examination.

With regard to noise characteristics, the $4k$ system appears to be unequivocally superior to the $2k$ system. The better NPS of the $4k$ system can in part be attributed to the increased laser reading time of the phosphor screen. Because of the overhead associated with data handling and electronic processes, we were unable to directly measure the actual laser scanning time of the screen. Instead, we measured the time elapsed from the appearance of the first row of image data on the acquisition monitor until the display of the last row of data. The values were 45 and 26 s for the $4k$ and the $2k$ acquisition modes, respectively. The increased scanning time may more efficiently extract the optical signals from the phosphor screen for the same level of deposited energy, which may lead to a less noisy output.

The reduced MTF at low and midfrequencies and the decreased NPS observed for the $4k$ mode as compared to that for the $2k$ mode may also be attributed to the signal processing applied to the $2k$ image, which has led to improved resolution at the expense of noise. The FCR-9501/FCR-9501-HQ imaging system is understood to scan the phosphor plate and sample the optical signal at a rate higher than the sampling rate of the image.[21,22] The finely sampled signals are processed to form the final image. This signal processing, similar to image enhancement algorithms, is expected to enhance the frequency content of the image at the expense of a higher level of noise. Further evidence for the influence of this preprocessing step is the physical performance of the $4k$-reduced mode of the system discussed below.

One way of acquiring $2k$ images with improved noise characteristics is to initially scan the phosphor in the $4k$ mode and then reduce the $4k$ image to $2k$ by an option in the configuration setup of the system's quality assurance workstation (HIC-654). We also assessed the image quality of these $4k$-reduced images. Figure 13 shows the MTF, NPS, and DQE for the $2k$, $4k$, and $4k$-reduced modes in the plate-scan direction at 115 kV$_p$. The presampled MTF for the $4k$-reduced mode is similar to that for the $4k$, but it falls lower as frequency increases, approaching a MTF of zero at about 5 cycles/mm. The NPS measures of these two modes are also similar, with that of the $4k$-reduced being slightly higher at low frequencies and aliased as it approaches f_N at
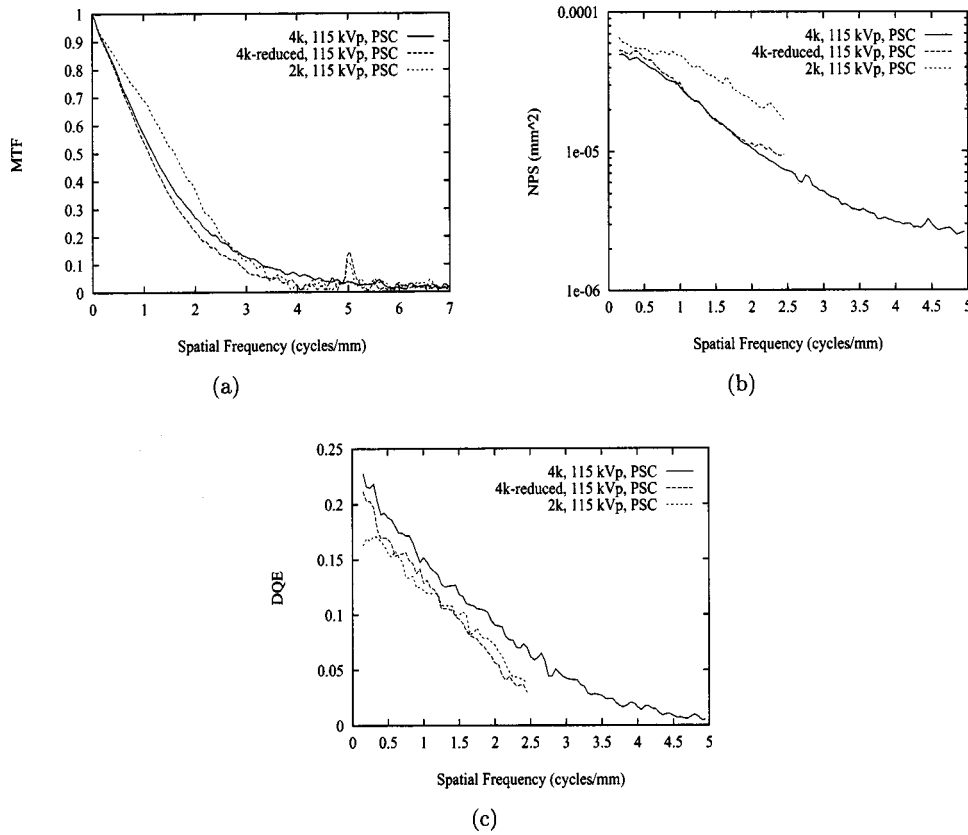
FIG. 13. The presampled MTF (a), NPS (b), and DQE (c) for the $4k$, $4k$-reduced, and $2k$ modes in the plate-scan direction acquired at 115 kV$_p$.

2.5 cycles/mm. The overall DQE of the $4k$-reduced mode is slightly lower than that of the $4k$ by about 0.01, and is close to that of the $2k$. Similar observations were made in the laser-scan direction. Based on these observations, the $4k$-reduced mode may be considered a good solution for acquiring $2k$ chest images with noise characteristics better than the standard $2k$-acquired images without running into the image-handling and storage difficulties associated with large $4k$ images. However, the resolution response in the low- to midfrequency range would be compromised, and throughput of the system would be similar to that of a $4k$ system.

To our knowledge there have been no published data on image quality measures on the FCR-9501/FCR-9501-HQ system. However, there have been several recent publications on the performance of other DSP systems. Dobbins et al. reported on the performance of four generations of DSP systems.[7] The most recent system that they evaluated is the PCR-7000 (Phillips Medical Systems) whose performance may be compared with our results for the FCR-9501 $2k$ system. The DQE measure for the PCR-7000 system is higher than our results for the the FCR-9501 system [Fig. 11(b)] by approximately 0.05 at zero frequency. The frequency dependencies are otherwise similar. Many factors

TABLE II. Some factors that contribute to the differences between the current measurements and those reported by Dobbins et al. (Ref. 7) and Kengyelics et al. (Ref. 21).

	Dobbins et al. (Ref. 7)	Kengyelics et al. (Ref. 21)	Current method
DSP reader	Phillips PCR-7000	Phillips PCR AC3	Fuji FCR-9501 (HQ)
Stimulation laser	Helium–neon/633 nm	Solid-state/680 nm	Solid-state/680 nm
Reflective mirror	Single oscillating	Rotating polygon	Rotating polygon
ADC	10 bit[a]	12 bit	12 bit
Phosphor screen	ST-V	ST-V	ST-Va
Delay time	10 min	10 min	<0.5 min (automated)
kV$_p$ setting	70 kV$_p$	75 kV$_p$	70 kV$_p$
Filtration	0.5 mm Cu	1.5 mm Cu	19 mm Al
HVL	Not reported	0.5 mm Cu	6.3 mm Al
Ideal SNR^2/mR	2.70×10^5 #/mm^2 mR[b]	3.10×10^5 #/mm^2 mR[c]	2.62×10^5 #/mm^2 mR

[a]Prescanning required.
[b]Provided by the manufacturer.
[c]Using 0.873 rad/R.

may contribute to this difference, some of which are listed in Table II. In addition, exposure measurement accuracy and differences in the details of the measurement techniques (e.g., the method for obtaining the ideal SNR, details of the processing steps for derivation of the NPS) complicate a direct comparison of the results.

Recently, Kengyelics, Launders, and Cowen reported their assessment of the PCR AC3 system (Phillips Medical Systems).[21] Their results for a 100 μm pixel size indicated a lower DQE than our assessment for the FCR-9501-HQ system [Fig. 11(a)] by about 0.05 at zero frequency. The PCR AC3 system uses an internal reading engine very similar to the FCR-9501/FCR-9501-HQ system. However, the systems have different mechanical configurations. Some other factors that may contribute to observed differences are listed in Table II. It should be noted that similar to the former comparison, exposure measurement accuracy and differences in the measurement method contribute to the observed deviations. It should also be noted that in both previous studies, ST-V phosphor screens were employed. In this work, we used the next generation of DSP phosphor screens, ST-Va, which has an extended protective layer compared to ST-V screens to minimize surface cracking caused by extensive use.

Our method for measuring the system MTF employs an edge phantom rather than a slit phantom as employed by Dobbins *et al.*[7] and by Kengyelics, Launders, and Cowen.[21] In a previous paper, we reported a detailed comparison of MTF measurement methods using edge and slit phantoms.[11] For low frequencies, the edge method was found to provide more accurate results due in part to the uncertainty in methods used to extrapolate tails of the line spread function measured with a slit phantom. The methods were otherwise shown to be essentially equivalent.

Our method for measuring the NPS is somewhat different from those reported by other authors. A two-dimensional Fourier transform method is used similar to that reported by Dobbins *et al.* Additional analysis steps used in the method we report here are:

(1) A two-dimensional function is used to correct for low-frequency image variations due to the x-ray source heel effect or to electronic drift.

(2) A spectral estimation window function is used to reduce low-frequency artifacts and reduce the noise in the spectrum.

(3) The spectral values in each subarray are corrected for exposure differences in the radiographic field relative to the position of an ion chamber.

Spectral averaging of the estimate from many small subarrays is required to obtain low noise in the NPS. Since the NPS does not usually have a fine structure, we have used small subarray sizes and additional spectral smoothing from the window function. In Fig. 12, some peaks in the spectrum obtained with a high exposure are observed, which probably reflect narrow-band noise for which the width reflects the resolution in our spectral estimation. Further reduction in NPS estimation noise might be obtained by using overlapped blocks[23,24] and by restricting the analysis to the laser-scan

and the plate-scan directions by projecting the data within the subarrays and utilizing a one-dimensional transform.[24]

The above comparisons demonstrate the difficulty in comparing the results of the MTF, NPS, and DQE measurements from different laboratories. Similar measurement methodologies should be utilized if different systems are to be compared. In a previous study, we compared the performance of the Fuji FCR-9501/FCR-9501-HQ system with that of the Kodak KESPR-400 system using the same measurement methods.[20] The results of that study indicated that for standard-resolution screens under similar experimental conditions, comparable systems from the two manufacturers have similar signal, noise, and signal-to-noise transfer characteristics, while high-resolution screens provide improved resolution with an adverse effect on noise. This paper similarly concluded that the resolution of DSP systems is mainly limited by the optical properties of the screen, which were similar for the two systems.

V. CONCLUSION

The intrinsic image quality of a $4k$ and a $2k$ digital storage phosphor chest radiographic system was determined by measuring the MTF, NPS, and DQE of the systems. The results indicate that the $4k$ system is slightly better with respect to noise characteristics. However, the resolution response of the $4k$ system is inferior to that of the $2k$ system in the low- to midfrequency range. In terms of the DQE, the $4k$ system offers slightly better signal-to-noise characteristics when compared to the $2k$ system. Overall, the physical performance of the $4k$ system is not significantly better than that of the $2k$ system. Recent clinical comparisons confirm this conclusion.[22]

APPENDIX

Image noise is commonly interpreted as being equivalent to the noise produced by a detector which counts input quanta. If the number of counted quanta vary with a Poisson distribution and are spatially uncorrelated, the variance of the noise in a uniform image equals the average number of quanta counted per pixel. In this work, the measured relative image noise variations were multiplied by the square root of the pixel area [see Eq. (7)] such that $\delta'_s(j,k)$ has units of mm and the relative noise variance has been interpreted as $1/(\text{quanta/mm}^2)$. We consider first how the NPS is deduced from $\delta'_s(j,k)$ without application of the window function used for spectral estimation [i.e., Eq. (8) for $\delta''_s(j,k)$].

The fast Fourier transform (FFT) computer algorithm used in this work was equivalent to

$$\text{FFT}(\delta'_s(j,k)) = \sum_{j=1}^{N} \sum_{k=1}^{N} \delta'_s(j,k) e^{-i2\pi((n/N)j+(m/N)k)}.$$

(A1)

When Fourier transformation integrals are transformed to a discrete form, the differential elements of the integration lead to terms for Δx and Δy within the summation. Most numeric FFT algorithms are equivalent to Eq. (A1) and do not include these terms. Since they are application specific, it is assumed

that they will be applied as needed elsewhere in the analysis. The discrete Fourier transformation is thus written as

$$\mathcal{F}(\delta'_s(j,k)) = a_p \text{FFT}(\delta'_s(j,k)), \tag{A2}$$

where we associate the pixel area $a_p = x_p y_p$ with $\Delta x \Delta y$. The operator $\mathcal{F}(\cdots)$ results in a two-dimensional array whose elements have complex values. From Eqs. (A1) and (A2), it can easily be seen that the units of $\mathcal{F}(\delta'_s(j,k))$ are that of $\delta'_s(j,k)$ time the units of a_p, and thus, mm^3.

The correct magnitude of the NPS is established in part by Parseval's theorem which equates the total noise power in both the spatial and the frequency domains. The discrete Parseval's theorem may be written as

$$\sum_{j=1}^{N} \sum_{k=1}^{N} [\delta'_s(j,k)]^2 \Delta x \Delta y = \sum_{n=1}^{N} \sum_{m=1}^{N} |\mathcal{F}(\delta'_s(j,k))|^2 \Delta f_x \Delta f_y. \tag{A3}$$

In the frequency domain, the discrete frequency increments are $\Delta f_x = 1/X_p$ and $\Delta f_y = 1/Y_p$, where X_p and Y_p are the spatial dimensions of the original image; $X_p = N x_p$, $Y_p = N y_p$. The equation resulting from Parseval's theorem thus reduces to

$$\sum_{j=1}^{N} \sum_{k=1}^{N} [\delta'_s(j,k)]^2 = \frac{1}{N^2 a_p^2} \sum_{n=1}^{N} \sum_{m=1}^{N} |\mathcal{F}(\delta'_s(j,k))|^2. \tag{A4}$$

Equation (A4) can be rewritten in terms of the variance of the scaled relative image noise, $\sigma_{\delta'}^2$, which from Eq. (7) is equal to $a_p \sigma_\delta^2$. Using Eq. (5) for σ_δ^2, Eq. (A4) becomes

$$\sigma_{\delta'}^2 = \frac{1}{N^4 a_p^2} \sum_{n=1}^{N} \sum_{m=1}^{N} |\mathcal{F}(\delta'_s(j,k))|^2. \tag{A5}$$

Since $\mathcal{F}(\delta'_s(j,k))$ has units of mm^3, this results in the expected units of mm^2 for $\sigma_{\delta'}^2$.

The noise power spectrum has been conventionally defined such that all of the elements corresponding to very low spatial frequency (i.e., n and m small) have a value equal to 1/NEQ. This in turn is equal to the relative noise variance that would be observed for uncorrelated noise as was noted in Eq. (6). Considering Eq. (A5) we define the noise spectrum as

$$\eta_s(n,m) = \frac{1}{N a_p} \mathcal{F}(\delta'_s(j,k)) = \frac{1}{N} \text{FFT}(\delta'_s(j,k)), \tag{A6}$$

and the noise power spectrum as the squared magnitude of the complex values of the noise spectrum

$$\text{NPS}_s(n,m) = |\eta_s(n,m)|^2. \tag{A7}$$

By defining $\delta'_s(j,k)$ as we have with units of mm [Eq. (7)], the appropriate units are obtained for the NPS by using only the simple relationships in Eq. (A6) and (A7). Specifically, the units of $\eta_s(n,m)$ are mm and the units of NPS are mm^2, which is interpreted as mm^2 per quanta.

Using these definitions, the equation resulting from Parseval's theorem becomes

$$\sigma_{\delta'}^2 = \frac{1}{N^2} \sum_{n=1}^{N} \sum_{m=1}^{N} \text{NPS}_s(n,m). \tag{A8}$$

The observed relative noise variance is thus simply equal to the average value of the noise power spectrum. This simple relationship is often suggested to confirm the values of the noise power spectrum by estimating the variance of the noise in an image and then scaling by the pixel area to obtain $\sigma_{\delta'}^2$. For uncorrelated noise, the NPS is approximately constant for all elements and each element value is approximately equal to $\sigma_{\delta'}^2$.

In this work we have used a window function to avoid aliasing and provide some smoothing of the estimated NPS. This has been applied as a multiplication in the spatial domain of $\sigma_{\delta'}^2$ to obtain $\sigma_{\delta''}^2$ and has the effect of a convolution in the frequency domain of the NPS. The absolute values of the NPS are not changed as long as the total power of the window function in the frequency domain is 1.0. This is achieved by normalizing the window function such that the mean-square sum in the spatial domain is 1.[25] Thus, no further normalization is required when deducing $\text{NPS}_s(n,m)$ from $\delta''_s(j,k)$.

a)This work was presented in part at the joint meeting of the American Association of Physicists in Medicine and the Radiological Society of North America, Chicago, Illinois, December 1996.

b)Electronic mail: mikef@rad.hfh.edu

c)Currently located at the Medical University of South Carolina, Charleston, SC.

[1] J. T. Dobbins, D. L. Ergun, H. Blume, and L. J. Rutz, ''Detective quantum efficiency of three generations of computed radiography acqusition systems,'' Radiology **185**, 159 (1992).

[2] W. Hillen, U. Schiebel, and T. Zaengel, ''Imaging performance of a digital storage phosphor system,'' Med. Phys. **14**, 744–751 (1987).

[3] H. Fujita, D.-Y. Tsai, T. Itoh, K. Doi, J. Morishita, K. Ueda, D. Y. Tsai, and A. Ohtsuka, ''A simple method for determining the modulation transfer function in digital radiography,'' IEEE Trans. Med. Imaging **11**, 34–39 (1992).

[4] H. Fujita, K. Ueda, J. Morishita, T. Fujikawa, A. Ohtsuka, and T. Sai, ''Basic imaging properties of a computed radiographic system with photostimulable phosphors,'' Med. Phys. **16**, 52–59 (1989).

[5] H. Fujita, J. Morishita, K. Ueda, D. Y. Tsai, A. Ohtsuka, and T. Fujikawa, ''Resolution properties of a computed radiographic system,'' SPIE Med. Imaging **1090**, 263–275 (1989).

[6] T. Matsuda, S. Arakawa, K. Kohda, S. Torii, and N. Nakajima, ''New technological developments in the FCR9000,'' Fuji Computed Radiography, Technical Review 2, Fuji Photo Film Co., Ltd., 1993.

[7] J. T. Dobbins, D. L. Ergun, L. Rutz, D. A. Hinshaw, H. Blume, and D. C. Clark, ''DQE(f) of four generations of computed radiography acquisition devices,'' Med. Phys. **22**, 1581–1593 (1995).

[8] K. Doi, P. C. Bunch, G. Holje, M. Pfeiler, and R. F. Wagner, *Modulation Transfer Function of Screen–Film Systems*, ICRU 41, International Commission on Radiation Units and Measurements, Bethesda, MD, 1986.

[9] J. Morishita, K. Doi, R. Bollen, P. C. Bunch, D. Hoeschen, G. Sirand-Rey, and Y. Sukenobu, ''Comparison of two methods for accurate measurement of modulation transfer functions of screen–film systems,'' Med. Phys. **22**, 193–200 (1995).

[10] K. Doi, J. Holje, L.-N. Loo, H.-P. Chan, J. M. Sandrick, R. J. Jennings, and R. F. Wagner, *MTF's and Wiener Spectra of Radiographic Screen–Film Systems* (U.S. HHS, FDA, Rockville, MD, 1982), Vol. 1, No. 82–8187.

[11] E. Samei, M. J. Flynn, and D. A. Reimann, ''A method for measuring the presampled MTF of digital radiographic systems using an edge test device,'' Med. Phys. **25**, 102–113 (1998).

[12] J. Morishita, H. MacMahon, K. Doi, M. Carlin, and Y. Sukenobu,

''Evaluation of an asymmetric screen–film system for chest radiography,'' Med. Phys. **21**, 1769–1775 (1994).

[13]M. L. Giger, K. Doi, and C. E. Metz, ''Investigation of basic imaging properties in digital radiography. 1. Noise Wiener spectrum,'' Med. Phys. **11**, 797–805 (1984).

[14]R. J. Jennings, H. Jafroudi, R. M. Gagne, T. R. Fewell, P. W. Quinn, D. E. Steller Artz, J. J. Vucich, M. T. Freedman, and S. K. Mun, ''Storage-phosphor-based digital mammography using a low-dose x-ray system optimized for screen–film mammography,'' SPIE Med. Imaging **2708**, 220–232 (1996).

[15]J. C. Dainty and R. Shaw, *Image Science* (Academic, New York, 1974).

[16]W. K. Pratt, *Digital Image Processing* (Wiley, New York, 1991).

[17]J. T. Dobbins, ''Effects of undersampling on the proper interpretation of modulation transfer function, noise power spectra, and noise equivalent quanta of digital imaging systems,'' Med. Phys. **22**, 171–181 (1995).

[18]E. Storm, ''Calculated bremsstrahlung spectra from thick tungsten targets,'' Phys. Rev. A **5**, 2328–2338 (1971).

[19]E. Storm, ''Emission of characteristic *L* and *K* radiation from thick tungsten targets,'' J. Appl. Phys. **43**, 2790–2796 (1972).

[20]E. Samei, M. J. Flynn, and W. R. Eyler, ''Simulation of subtle lung nodules in projection chest radiography,'' Radiology **202**, 117–124 (1997).

[21]S. M. Kengyelics, J. H. Launders, and A. R. Cowen, ''Physical imaging performance of a compact computed radiography acquisition device,'' Med. Phys. **25**, 354–360 (1998).

[22]H. MacMahon, J. H. Lee, K. Hoffmann, M. Carlin, and K. Doi, ''Comparison of high-resolution and standard-resolution digital chest radiographs with an asymmetric screen–film system,'' Radiology **201**, 400 (1996).

[23]F. J. Harris, ''On the use of windows for harmonic analysis with the discrete Fourier transform,'' Proc. IEEE **66**, 51–83 (1978).

[24]E. Muka, T. Mertelmeier, R. M. Stone, and E. Senol, ''Impact of image noise and phosphor granularity on the specification of high-resolution medical image CRT displays,'' SPIE Med. Imaging **3031**, 210–221 (1997).

[25]W. H. Press, S. A. Teukolsky, W. T. Vetterling, and B. P. Flannery, *Numerical Recipes in C* (Cambridge University Press, New York, 1992).